

Evolutionary search for cobalt-rich compounds in the yttrium-cobalt-boron system

Takahiro Ishikawa,^{1,*} Taro Fukazawa,^{2,1} Guangzong Xing,¹ Terumasa Tadano,^{3,1} and Takashi Miyake^{2,1}

¹*ESICMM, National Institute for Materials Science, 1-2-1 Sengen, Tsukuba, Ibaraki 305-0047, Japan*

²*CD-FMat, National Institute of Advanced Industrial Science and Technology,
1-1-1 Umezono, Tsukuba, Ibaraki 305-8568, Japan*

³*CMSM, National Institute for Materials Science, 1-2-1 Sengen, Tsukuba, Ibaraki 305-0047, Japan*

(Dated: February 4, 2021)

Modern high-performance permanent magnets are made from alloys of rare earth and transition metal elements, and large magnetization is achieved in the alloys with high concentration of transition metals. We applied evolutionary search scheme based on first-principles calculations to the Y-Co-B system and predicted 37 cobalt-rich compounds with high probability of being stable. Focusing on remarkably cobalt-rich compounds, YCo₁₆ and YCo₂₀, we found that, although they are metastable phases, the phase stability is increased with increase of temperature due to the contribution of vibrational entropy. The magnetization and Curie temperature are higher by 0.22 T and 204 K in YCo₁₆ and by 0.29 T and 204 K in YCo₂₀ than those of Y₂Co₁₇ which has been well studied as strong magnetic compounds.

PACS numbers: 61.50.Ah, 75.50.Bb, 75.50.Cc, 75.50.Ww

I. INTRODUCTION

Rare-earth magnets are strong permanent magnets, which mainly consist of rare-earth elements and 3d transition metals (Fe and/or Co). High Fe/Co concentration gives rise to high magnetization and rare earths are a source of high magnetocrystalline anisotropy which is essential for high coercivity. Rare-earth magnets have been developed since the discovery of large magnetocrystalline anisotropy in an alloy of yttrium and cobalt, YCo₅¹, and neodymium magnets are the strongest type of permanent magnet commercially available, and its main phase is formed by Nd₂Fe₁₄B compound², which has the saturation magnetization of 1.85 T at 4.2 K, magnetocrystalline anisotropy field of 5.3 MA/m at room temperature, and Curie temperature of 586 K³.

The magnetization is expected to be further increased using iron-richer compounds than Nd₂Fe₁₄B, and RT_{12} (R = rare earth; T = Fe, Co) systems have attracted considerable attention as potential candidates for stronger permanent magnets than Nd₂Fe₁₄B⁴⁻⁶. It has long been known that RT_{12} compounds are thermodynamically unstable in a bulk form and are stabilized by partial substitution of the third element for T , *i.e.* $R(T_{1-x}X_x)_{12}$ (X = Al, Si, Ti, V, Cr, Nb, Mo, W)⁷⁻¹³. However, the magnetization decreases with the increase of x , and a search is currently underway for the best third elements, in other words, the elements maximizing the stabilization and minimizing the decrease of the magnetization. On the other hands, thin films of NdFe₁₂N _{x} and Sm(Fe_{1- x} Co _{x})₁₂ have been fabricated by the epitaxial growth on W- and V-buffered MgO(001) substrates. The films have higher magnetization, Curie temperature, and anisotropy field than Nd₂Fe₁₄B^{14,15}. In addition, YFe₁₂ with the ThMn₁₂ structure is experimentally obtained in multi-phases by rapid quenching method¹⁶. Recently, first-principles calculations predict that, in YFe₁₂ and Y(Fe_{1- x} Co _{x})₁₂ with x of 0–0.7, the magnetization and Curie temperature are

enhanced by the transformation from ThMn₁₂ into monoclinic $C2/m$ structures¹⁷.

In the present study, we search for novel stable compounds with novel Fe/Co-rich rare-earth compounds using composition and crystal structure prediction scheme based on first-principles calculations and evolutionary algorithm. Here, we focused on Y-Co-B system for the following reasons: (i) Y is favorable for theoretical treatment because it has no f electron in its ground-state electronic configuration, (ii) Co has a hexagonal close-packed (hcp) structure in the simple substance and is expected to be compatible with Y having hcp compared with Fe having a body-centered cubic structure, which makes a wide variety of compositions stable, and (iii) B can play a role for stabilizing Y-Co compounds and forming novel crystal structures, similarly to the case of Nd₂Fe₁₄B. As a result, we found 37 cobalt-rich compounds including remarkably Co-rich YCo₁₆ and YCo₂₀.

II. COMPUTATIONAL DETAILS

We used the evolutionary construction scheme of a formation-energy convex hull¹⁸ to search for stable compounds in the Y-Co-B system. First, we created an initial set of Y-Co-B compounds using the structure data of experimentally reported YFe₃, Y₆Fe₂₃, Y₃Fe₂₉, NdFe₂, NdFe₅, Nd₂Fe₁₇, Sm₅Fe₁₉, YB₂, YB₄, CoB, YCo₂B₂, Y₄CoB₁₃, Nd₂Fe₁₄B, Sm₂Fe₁₇N₃, and SmCo₃B₂, which are included in the Materials Project database¹⁹ and the SpringerMaterials database²⁰. For the pure elements, we used the hcp structures for Co and Y, and a rhombohedral $R\bar{3}m$ structure for B. Next, we constructed the preliminary convex hull of Y-Co-B system by performing the structural optimizations for the compounds in the initial set. Then, by applying evolutionary operators, “mating”, “mutation”, and “adaptive mutation”¹⁸ to target compounds selected from the compounds whose

distance to the convex hull is small (0–4.4 mRy/atom), new compositions and structures with high probability of being stable were created. Repeatedly performing the creation of compounds and the update of the convex hull, we searched for stable compounds.

We combined our evolutionary construction code with the Quantum ESPRESSO (QE) code²¹ to perform the optimizations of the structures created by the operators. We used the generalized gradient approximation by Perdew, Burke and Ernzerhof (PBE) for the exchange-correlation functional in the framework of the projector augmented wave (PAW) method²². We got the PAW potentials from the QE web site²³. The energy cutoff was set at 100 Ry for the wave function and 800 Ry for the charge density. The maximum number of atoms in calculation cell is 84, and the k -space integration over the Brillouin zone (BZ) was carried out on $12 \times 12 \times 12$, $8 \times 8 \times 8$, $6 \times 6 \times 6$, and $4 \times 4 \times 4$ grids for the structures including 1–4, 5–12, 13–30, and more than 30 atoms in the calculation cell, respectively.

To investigate dynamical and thermodynamical stability of the predicted compounds, we calculated phonon dispersion and vibrational free energy using the Vienna *ab initio* simulation package (VASP)²⁴ and the PHONOPY code²⁵. Second-order interatomic force constants were computed by the finite-displacement method based on harmonic approximation, as implemented in PHONOPY. Total number of atoms in each supercell is ~ 100 or larger, which was sufficient to reach the convergence of the vibrational free energy. The energy cutoff for the wave function was set at 400 eV, and the k -point mesh was generated automatically in such a way that the mesh density in the reciprocal space is larger than 450 \AA^{-3} . The convergence criteria of energy and force minimization were set to 10^{-8} and 10^{-7} eV, respectively.

For the stable compounds, we calculated the intersite magnetic couplings using the Liechtenstein’s method²⁶. For this purpose, we used AkaiKKR²⁷, a first-principles program of Korringa-Kohn-Rostoker (KKR) Green’s function method, within the local density approximation. The Curie temperature T_C is evaluated from a classical spin model within the mean-field approximation. Other computational details are the same to the settings in Ref. 28.

III. RESULTS

In this study, we searched for stable and metastable compounds with the convex-hull distance ΔE less than 4.4 mRy/atom (59.8 meV/atom). This tolerance is associated with the approximations and the omission of temperature effects in first-principles calculations^{29,30}, and the possibility of the stabilization by inclusion and/or substitution of other elements. We created 4120 structures up to the 11th generation by applying the evolutionary construction technique to the Y-Co-B system ($Y_{1-x-y}Co_xB_y$, $0 \leq x \leq 1$, $0 \leq y \leq 1$) and pre-

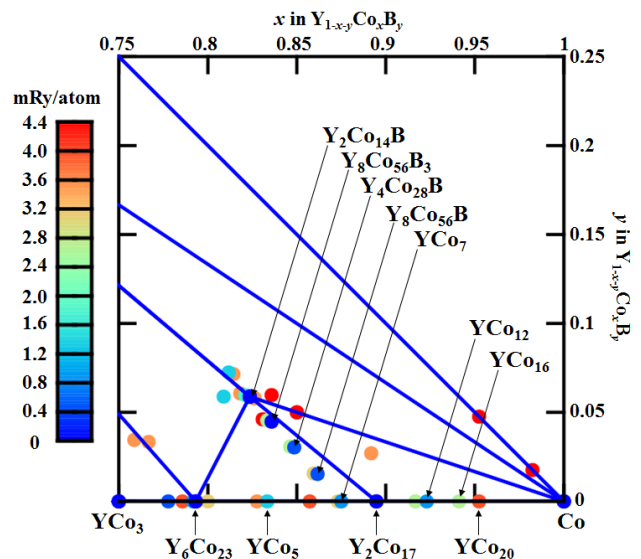


FIG. 1: Projection of the formation-energy convex hull of $Y_{1-x-y}Co_xB_y$ on the xy plane. The solid lines are the edges of the convex hull, and the dots show the compounds with the convex-hull distance less than 4.4 mRy/atom.

dicted Y_3Co , YCo , YCo_2 , YCo_3 , Y_6Co_{23} , Y_2Co_{17} , YB_2 , YB_3 , CoB , YCo_2B_2 , YCo_3B_2 , and $Y_2Co_{14}B$ as stable compounds on the convex hull (See Fig. S1 in Supplemental Material [SM]³¹). Figure 1 shows the closeup of the convex hull in the Co-rich region of $0.75 \leq x \leq 1$, in which we found four stable and 33 metastable compounds. The most important observation here is that YCo_{16} and YCo_{20} emerge as Co-richer compounds than YCo_{12} . The ΔE values are 2.72 mRy/atom for YCo_{16} and 3.92 mRy/atom for YCo_{20} . In addition, for the metastable YCo_5 phase, we obtained an orthorhombic *Imma* structure, which is more stable by 0.27 mRy/atom than the $CaCu_5$ -type structure used to construct the preliminary convex hull (See Fig. S8 and Table S7 in SM for the details of the structure³¹). Another important point is that $Y_2Co_{14}B$ transforms into YCo_7 with an ordered tetragonal structure $P4_2/mnm$, going through the small energy region of ΔE less than 0.82 mRy/atom. $Y_2Co_{14}B$ takes the $Nd_2Fe_{14}B$ -type structure with $P4_2/mnm$ including four formula units in the unit cell. The low-energy path connecting between $Y_2Co_{14}B$ and YCo_7 is achieved by step-by-step eliminating the B atoms from the unit cell (See Fig. S30 in SM³¹). See Fig. S2 in SM for the details of other metastable compounds³¹.

Hereafter, we focus on the novel Co-rich compounds, YCo_{16} and YCo_{20} . The structures are assigned as triclinic $P\bar{1}$ for YCo_{16} and monoclinic $C2/m$ for YCo_{20} (See Tables S27 and S28 and Fig. S28 and S29 in SM for the details of the structures³¹). Figure 2 shows $I4/mmm$ ($ThMn_{12}$ -type) YCo_{12} viewed along the b axis, $P\bar{1}$ YCo_{16} viewed along the $[1\bar{1}0]$ direction, and $C2/m$ YCo_{20} viewed along the b axis. $P\bar{1}$ YCo_{16} and $C2/m$ YCo_{20} are achieved by adding the Co atoms into $ThMn_{12}$ -type

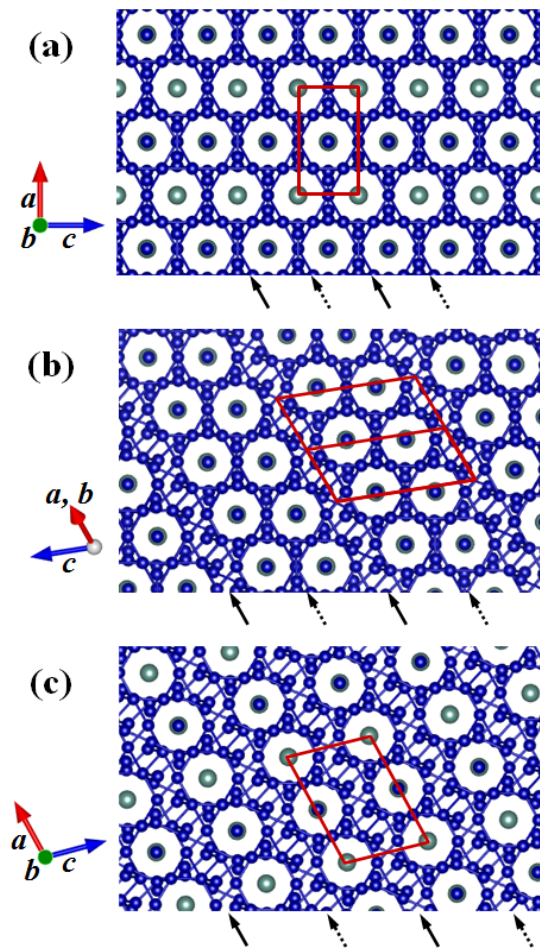


FIG. 2: Projections of (a) YCo_{12} with a tetragonal $I4/mmm$ (ThMn₁₂-type) structure along the b axis, (b) YCo_{16} with a triclinic $P\bar{1}$ structure along the $[1\bar{1}0]$ direction, and (c) YCo_{20} with a monoclinic $C2/m$ structure along the b axis. Frames show the unit cells, and large and small balls represent the Y and Co atoms, respectively. The solid (broken) arrows show the areas where additional Co atoms are inserted by the transformation from YCo_{12} (YCo_{16}) into YCo_{16} (YCo_{20}). Crystal structures were drawn with VESTA³².

YCo_{12} . YCo_{16} (YCo_{20}) is obtained by the insertion of the four Co atoms per formula unit into the area shown by the solid (broken) arrows of YCo_{12} (YCo_{16}), parallel to the (101) plane of ThMn₁₂-type YCo_{12} .

We investigated the dynamical and thermodynamical stability of YCo_{16} and YCo_{20} by performing phonon calculations. Figure 3 shows the phonon dispersion curves of $P\bar{1}$ YCo_{16} and $C2/m$ YCo_{20} . No imaginary phonon modes were detected in the dispersion curves, which indicates that the two structures are dynamically stable at 0K. We investigated the variations of the convex-hull distance for YCo_{16} and YCo_{20} with increase of temperature by considering the entropy contribution, including electronic and vibrational free energies (Fig. 4). We compared the static formation energies of $I4/mmm$ YCo_{12} , $P\bar{1}$ YCo_{16} , and $C2/m$ YCo_{20}

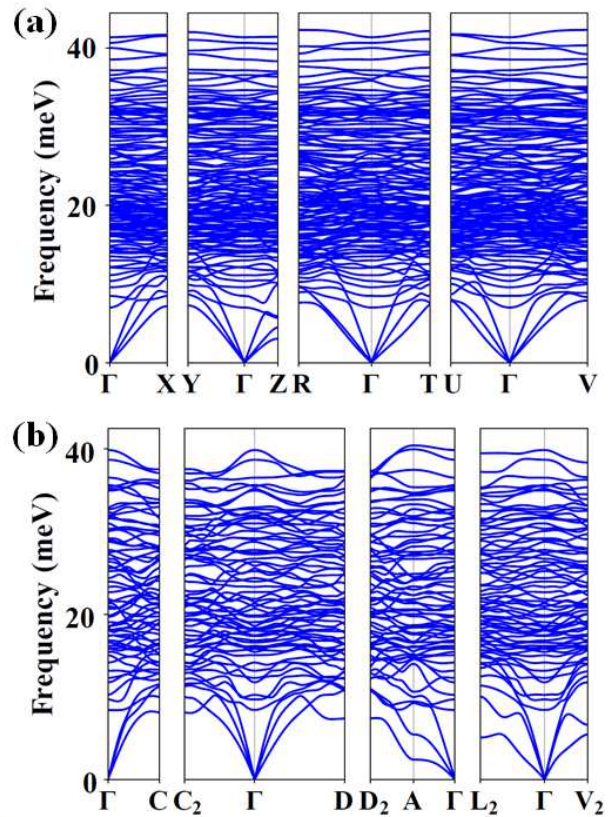


FIG. 3: Phonon dispersions of (a) YCo_{16} with a triclinic $P\bar{1}$ structure and (b) YCo_{20} with a monoclinic $C2/m$ structure.

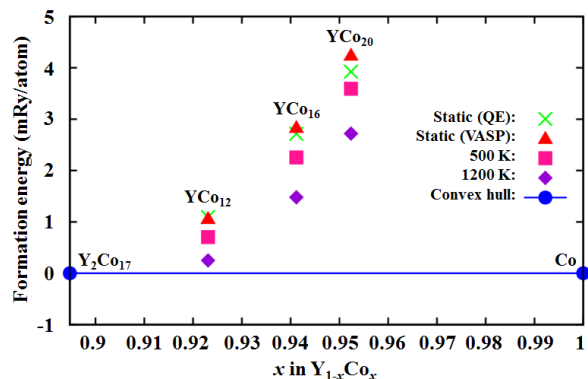


FIG. 4: Phase stability of YCo_{12} , YCo_{16} , and YCo_{20} against the decomposition into Y_2Co_{17} and Co.

between QE and VASP and confirmed the errors are 0.03 mRy/atom, 0.12 mRy/atom, and 0.32 mRy/atom, respectively. Since these results are reasonably consistent with each other, we discuss the finite-temperature thermodynamic stability of YCo_{16} and YCo_{20} based on the VASP results. With increasing the temperature up to 1200 K, the convex-hull distances decrease to 0.25 mRy/atom for YCo_{12} , 1.48 mRy/atom for YCo_{16} , and 2.72 mRy/atom for YCo_{20} . Regarding the struc-

TABLE I: Comparison of volume per atom V , magnetic moment per atom m , magnetization M , and Curie temperature T_C among Y_2Co_{17} , YCo_{12} , YCo_{16} , YCo_{20} , Y_2Fe_{17} , YFe_{12} , YFe_{16} , and YFe_{20} .

	structure	V ($\text{\AA}^3/\text{atom}$)	m (μ_B/atom)	M (T)	T_C (K)
Y_2Co_{17}	$R\bar{3}m$	12.60	1.354	1.252	1174
YCo_{12}	$I4/mmm$	12.15	1.455	1.396	1280
YCo_{16}	$P\bar{1}$	11.90	1.505	1.474	1378
YCo_{20}	$C2/m$	11.77	1.555	1.539	1378
Y_2Fe_{17}	$R\bar{3}m$	13.42	1.979	1.719	720
YFe_{12}	$I4/mmm$	12.88	2.019	1.826	792
YFe_{16}	$P\bar{1}$	12.65	2.093	1.928	719
YFe_{20}	$C2/m$	12.41	2.053	1.928	434

ture of Y_2Co_{17} , a rhombohedral $R\bar{3}m$ (Th_2Zn_{17} -type) structure is stable in the low-temperature region, while the entropy contributions make the hexagonal $P6_3/mmc$ (Th_2Ni_{17} -type) more stable at temperatures above 780 K. This temperature-induced phase transition was properly considered in the results shown in Fig. 4.

Next, we investigated the magnetic properties of $P\bar{1}$ YCo_{16} and $C2/m$ YCo_{20} . Table I lists volume per atom V , magnetic moment per atom m , total magnetization M , and Curie temperature T_C for Y_2Co_{17} , YCo_{12} , YCo_{16} , and YCo_{20} . The V and m values decrease and increase with the increase of the Co concentration, respectively. Consequently, the M value increases to 1.474 T in YCo_{16} and 1.539 T in YCo_{20} , which are larger than those in Y_2Co_{17} and YCo_{12} . Furthermore, we obtained that YCo_{16} and YCo_{20} show the T_C value of 1378 K, which is higher by 204 K and 98 K than those of Y_2Co_{17} and YCo_{12} , respectively. Although the mean-field approximation tends to overestimate T_C , the differences of theoretical T_C values among magnet compounds have been found to be qualitatively consistent with those in experiments^{28,33,34}. Therefore, we expect the trend of the enhancement in T_C is realistic.

We also calculated the V , m , M , and T_C values for Fe-based compounds. Although the m value increases with increase of the Fe concentration from Y_2Fe_{17} through YFe_{16} , it turns to the decrease in YFe_{20} due to the decrease of the magnetic moment of Fe at the 4e site. As a result, the M value shows the increase to 1.928 T in YFe_{16} , whereas there is no further increase in YFe_{20} . In contrast to the case of the Co-based compounds, the T_C value decreases to 719 K in YFe_{16} , which is almost equal

to that of Y_2Fe_{17} , and is largely decreased in YFe_{20} .

IV. CONCLUSION

In conclusion, we searched for stable compounds in the Y-Co-B system, $Y_{1-x-y}Co_xB_y$, using the evolutionary construction technique of a formation-energy convex hull. Focusing on Co-rich ($0.75 \leq x \leq 1$) and low energy ($\Delta H \leq 4.4$ mRy/atom) region, we predicted 34 compounds, including novel Co-rich compounds, YCo_{16} and YCo_{20} . In addition, we obtained a new stable structure of YCo_5 , and a low energy path connecting between $Y_2Co_{14}B$ and YCo_7 . Phonon calculations predict that YCo_{16} and YCo_{20} are dynamically stable and the hull distance ΔH is decreased to 1.48 mRy/atom for YCo_{16} and 2.72 mRy/atom for YCo_{20} with increase of temperature to 1200 K due to the contribution of the vibrational free energy. The calculated M and T_C values are 1.474 T and 1378 K in YCo_{16} and 1.539 T and 1378 K in YCo_{20} , which are larger than those in Y_2Co_{17} and YCo_{12} . We performed the same calculations for YFe_{16} and YFe_{20} , and obtained the results that, although the T_C values are decreased in YFe_{16} and YFe_{20} , the M values are increased.

This study provides novel Co-rich compounds, YCo_{16} and YCo_{20} , with high magnetization and high Curie temperature, whereas further studies are required to get the knowledge about their magnetocrystalline anisotropy and coercivity, which is crucial for the application of RT_{16} and RT_{20} systems to high-performance permanent magnet. For example, it is important to accumulate the data about the variation of the magnetocrystalline anisotropy and coercivity by systematically replacing Y with the other R elements.

Acknowledgments

This work was supported by the Ministry of Education, Culture, Sports, Science and Technology (MEXT) as ‘‘The Elements Strategy Initiative Center for Magnetic Materials (ESICMM)’’ (JPMXP0112101004) and ‘‘Program for Promoting Researches on the Supercomputer Fugaku’’ (DPMSD). The computation was partly conducted using the facilities of the Supercomputer Center, the Institute for Solid State Physics, the University of Tokyo, the supercomputer of ACCMS, Kyoto University, and the HPCI System Research project (Project ID:hp200125).

* Electronic address: ISHIKAWA.Takahiro@nims.go.jp

¹ G. Hoffer and K. Strnat, IEEE Trans. Magn. **2**, 487 (1966).

² M. Sagawa, S. Fujimura, H. Yamamoto, and Y. Matsuura, IEEE Trans. Magn. **20**, 1584 (1984).

³ S. Hirose, Y. Matsuura, H. Yamamoto, S. Fujimura, M. Sagawa, and H. Yamauchi, J. Appl. Phys. **59**, 873 (1986).

⁴ K. Ohashi, Y. Tawara, R. Osugi, and M. Shima, J. Appl.

- Phys. **64**, 5714 (1988).
- ⁵ K. H. J. Buschow, *J. Appl. Phys.* **63**, 3130 (1988).
 - ⁶ Y. Yang, L. Kong, S. Sun, D. Gu, and B. Cheng, *J. Appl. Phys.* **63**, 3702 (1988).
 - ⁷ I. Felner, I. Nowik, and M. Seh, *J. Magn. Magn. Mater.* **38**, 172 (1983).
 - ⁸ K. Ohashi, T. Yokoyama, R. Osugi, and Y. Tawara, *IEEE Trans. Magn.* **23**, 3101 (1987).
 - ⁹ K. Ohashi, Y. Tawara, R. Osugi, J. Sakurai, and Y. Komura, *J. Less-Common Met.* **139**, L1 (1988).
 - ¹⁰ D. B. D. Mooij and K. H. J. Buschow, *J. Less-Common Met.* **136**, 207 (1988).
 - ¹¹ B. Fuquana, J. L. Wang, O. Tegusa, W. Dagula, N. Tang, F. M. Yang, G. H. Wu, E. Brück, F. R. de Boer, and K. H. J. Buschow, *J. Magn. Magn. Mater.* **290-291**, 1192 (2005).
 - ¹² T. Miyake, K. Terakura, Y. Harashima, H. Kino, and S. Ishibashi, *J. Phys. Soc. Jpn.* **83**, 043702 (2014).
 - ¹³ Y. Harashima, K. Terakura, H. Kino, S. Ishibashi, and T. Miyake, *J. Appl. Phys.* **120**, 203904 (2016).
 - ¹⁴ Y. Hirayama, Y. K. Takahashi, S. Hirose, and K. Hono, *Scripta. Mater.* **95**, 70 (2015).
 - ¹⁵ Y. Hirayama, Y. K. Takahashi, S. Hirose, and K. Hono, *Scripta. Mater.* **138**, 62 (2017).
 - ¹⁶ H. Suzuki, *AIP Advances* **7**, 056208 (2017).
 - ¹⁷ T. Ishikawa, T. Fukazawa, and T. Miyake, *Phys. Rev. Materials* **4**, 104408 (2020).
 - ¹⁸ T. Ishikawa and T. Miyake, *Phys. Rev. B* **101**, 214106 (2020).
 - ¹⁹ A. Jain, S. P. Ong, G. Hautier, W. Chen, W. D. Richards, S. Dacek, S. Cholia, D. Gunter, D. Skinner, G. Ceder, et al., *APL Materials* **1**, 011002 (2013).
 - ²⁰ <https://materials.springer.com/>.
 - ²¹ P. Giannozzi, S. Baroni, N. Bonini, M. Calandra, R. Car, C. Cavazzoni, D. Cereso, G. L. Chiarott, M. Cococcioni, I. Dabo, et al., *J. Phys.: Condens. Matter* **21**, 395502 (2009).
 - ²² G. Kresse and D. Joubert, *Phys. Rev. B* **59**, 1758 (1999).
 - ²³ <https://www.quantum-espresso.org/>.
 - ²⁴ G. Kresse and J. Furthmüller, *Phys. Rev. B* **54**, 11169 (1996).
 - ²⁵ A. Togo and I. Tanaka, *Scripta Mater.* **108**, 1 (2015).
 - ²⁶ A. I. Liechtenstein, M. I. Katsnelson, V. P. Antropov, and V. A. Gubanov, *Journal of Magnetism and Magnetic Materials* **67**, 65 (1987).
 - ²⁷ AkaiKKR(Machikaneyama),
<http://kkk.issp.u-tokyo.ac.jp>, URL
<http://kkk.issp.u-tokyo.ac.jp>.
 - ²⁸ T. Fukazawa, H. Akai, Y. Harashima, and T. Miyake, *Journal of Physical Society of Japan* **87**, 044706 (2018).
 - ²⁹ Y. Wu, P. Lazic, G. Hautier, K. Persson, and G. Ceder, *Energy Environ. Sci.* **6**, 157 (2013).
 - ³⁰ Y. Hinuma, T. Hatakeyama, Y. Kumagai, L. A. Burton, H. Sato, Y. Muraba, S. Iimura, H. Hiramatsu, I. Tanaka, H. Hosono, et al., *Nat. Commun.* **7**, 11962 (2016).
 - ³¹ See Supplemental Material for formation energy convex hull, stable compounds, and their structure parameters.
 - ³² K. Momma and F. Izumi, *J. Appl. Crystallogr.* **44**, 1272 (2011).
 - ³³ T. Fukazawa, H. Akai, Y. Harashima, and T. Miyake, *Journal of Applied Physics* **122**, 053901 (2017).
 - ³⁴ T. Fukazawa, H. Akai, Y. Harashima, and T. Miyake, *IEEE Trans. Magn.* **55**, 2101305 (2019).